Applied Catalysis B: Environmental 96 (2010) 72–82

Contents lists available at ScienceDirect

Applied Catalysis B: Environmental

journal homepage: www.elsevier.com/locate/apcatb

Effect of sulfur as a growth promoter for CN_x nanostructures as PEM and DMFC ORR catalysts

Elizabeth J. Biddinger, Douglas S. Knapke, Dieter von Deak, Umit S. Ozkan *

Department of Chemical and Biomolecular Engineering, The Ohio State University, Columbus, OH, USA

ARTICLE INFO

Article history:
Received 4 July 2009
Received in revised form 24 January 2010
Accepted 1 February 2010
Available online 8 February 2010

Keywords:
Nitrogen-containing carbon
ORR catalysts
Fuel cell
Nanostructured carbon
Carbon growth promoters
Sulfur
CN_x

ABSTRACT

The impact of thiophene, a carbon growth promoter, was investigated when added to acetonitrile during pyrolysis over 2 wt%Fe/MgO to form nitrogen-containing carbon nanostructured (CN_x) oxygen reduction reaction (ORR) catalysts. ORR activity and selectivity were studied using rotating ring disk electrode (RRDE) electrochemical testing. Catalysts were characterized using XPS, TEM, hydrophobicity testing and BET surface area. It was found that thiophene did increase CN_x yield, but did not affect the ORR activity of the resulting catalysts. Characterization results revealed that sulfur was incorporated into the CN_x catalyst. Viability of catalysts for use in a PEM or direct methanol fuel cell environment was further investigated using temperature programmed oxidation and desorption (TPO, TPD) techniques to determine the stability of sulfur in CN_x catalyst. Post-synthesis treatment to prevent sulfur desorption during long-term use in a fuel cell was found to be feasible.

1. Introduction

Fuel cells are considered promising energy conversion devices to be used in the diversified energy portfolio of the future. Presently, capital costs for fuel cells are still significantly higher than the internal combustion engine and many batteries. A large part of the proton exchange membrane (PEM) and direct methanol fuel cell (DMFC) cost comes from the platinum catalysts, particularly at the cathode where the oxygen reduction reaction (ORR) is kinetically slow. Research attempts to decrease or eliminate the platinum in PEM and DMFC cathode catalysts are ongoing in many laboratories.

One family of alternate ORR catalysts being studied is the carbon-nitrogen catalysts. Carbon-nitrogen catalysts were first studied using macrocycles in the 1960s to mimic the hemoglobin-type active site [1,2]. While macrocycles were active for ORR, their stability was poor in the acidic environment of the fuel cells [3]. It was found that if these macrocycles were pyrolyzed or heat treated in an inert atmosphere at temperatures from 400 °C to 1000 °C they could maintain their activity while gaining stability [3–9]. More recently, non-macrocycle precursors have been used to create these carbon-nitrogen catalysts [10–18]. An example of the simple precursor catalyst would be a mixture of carbon black, iron acetate and ammonia being heat-treated together at elevated temperatures to form the catalyst [13]. The role of the metal, if any, in the resulting catalyst activity is still being debated in the literature [7,12,13,19–32].

Our work in this area involves the growth of nitrogen-containing carbon nanostructures (CN_x) catalysts from acetonitrile pyrolysis over various supports, including Vulcan carbon and metal oxides, with and without metal doping [33–39]. We have shown that ORR activity increases with the amount of stacked cup nanostructures found in the catalyst. Since stacked cup nanostructures have high edge plane exposure, there was also a correlation between edge plane exposure and ORR activity. In addition, trends in ORR activity with pyridinic-nitrogen content have also been found. Work with CN_x catalysts containing less than 1 ppm transition metals showed substantial ORR activity, indicating either iron was not part of the active site or that there were multiple possible active sites, one of which was metal-free, for CN_x catalysts [33].

Carbon-nitrogen catalysts reported in the literature, including our own work, have shown that while C-N catalysts have substantial activity for ORR, they were still not as active as platinum catalysts. Very recently, promising results involving carbon-nitrogen ORR catalysts have been published for both alkaline [40] and acidic systems [41] with comparable activity to the traditional platinum catalysts. Another advantage of these C-N

* Corresponding author. Tel.: +1 614 292 6623.
E-mail address: Ozkan.1@osu.edu (U.S. Ozkan).

0926-3373/$ – see front matter © 2010 Elsevier B.V. All rights reserved.
doi:10.1016/j.apcatb.2010.02.003

catalysts is their inactivity for methanol oxidation, making them attractive alternatives for direct methanol fuel cells.

As the activity of C-N catalysts continues to improve, manufacturing issues will have to be considered. If nanostructured carbons are to be used as fuel cell catalysts, then it is likely that their yield will have to be increased using a growth promoter in the energy-intensive manufacturing process. Sulfur has been reported as a growth promoter in the production of carbon nanofibers [42–47]. While reports discuss the benefits of low-levels of sulfur during the nanofiber growth-process, significant discussion on the presence of sulfur in the carbon nanostructures after production has not occurred. From these reports, it is unclear if sulfur remains in the carbon nanostructure and if so, whether it has an impact on the behavior of the nanostructure, especially in catalytic systems. The incorporation of sulfur into the graphitic nanostructure of carbon could alter the electronic behavior of the carbon, thereby changing the performance of carbon nanostructures used in electrochemical systems, such as ORR catalysts for PEM and DMFCs. Sulfur could also become a contaminant to different components of fuel cells if they were not well adhered to the catalyst.

In this study, we have investigated the use of thiophene as a growth promoter for the production of CN_x catalysts from acetonitrile pyrolysis and its impact on the catalyst behavior for the oxygen reduction reaction in a PEM or DMFC environment. It should be noted that, in this study, there was no effort made to optimize the catalyst formulation or the testing protocols to get the best performance since the focus of the paper is an understanding of the nature of the sulfur species incorporated during nanofiber growth and their impact on the ORR activity and selectivity.

2. Experimental methods

2.1. Materials preparation

The nanofiber growth catalyst used for the preparation of nitrogen-containing carbon nanostructures (CN_x) was 2 wt%Fe/MgO and was prepared using the incipient wetness impregnation technique. Iron (II) acetate (Sigma–Aldrich) and magnesia nanopowder from Sigma–Aldrich were used as the precursors. The nanofiber growth catalyst was dried at 110 °C in an atmospheric drying oven before fiber growth.

Acetonitrile (CH_3CN, Fisher, Optima grade) pyrolysis to form the CN_x catalyst was performed by placing 2 g of the 2 wt%Fe/MgO into a quartz boat inside a quartz tube in a high temperature furnace. Nitrogen at 150 mL/min was flowed through the tube while heating the furnace at 10 °C/min to 900 °C. Once 900 °C was reached, the N_2 stream was saturated with acetonitrile at room temperature by flowing through an acetonitrile bubbler and then fed to the furnace. The acetonitrile pyrolysis continued for 2 h at 900 °C followed by cooling in nitrogen.

Thiophene (C_4H_4S, Acros Organics) was added to the acetonitrile bubbler at levels of 1.8, 3.6, 5.5, 7.3, 8.9, 11.5 mol% as a growth promoter. For comparison, carbon nanostructures were also formed by pyrolyzing 100 mol% thiophene over the same fiber growth catalysts. All catalysts in this study are reported using the mol% thiophene in the acetonitrile solution, e.g., $CN_x(7.3)$ denotes CN_x catalysts prepared from a 7.3% thiophene in acetonitrile mixture. CS_y refers to the carbon nanostructures grown using thiophene only.

Weight gain due to CN_x (or CS_y) formation was calculated by comparing the mass of the 2 wt%Fe/MgO precursor, adjusted for mass loss during heating in N_2 to 900 °C, to the mass of the sample post-pyrolysis.

All carbon nanostructures were washed in 2.4 M HCl at 60 °C, vacuum filtered with excess deionized and distilled water and dried in an atmospheric oven at 110 °C to remove the magnesia support and any exposed iron.

2.2. Nitrogen physisorption

Nitrogen physisorption experiments to determine BET surface area and BJH pore volume were performed using a Micromeritics ASAP 2010.

2.3. Transmission electron microscopy (TEM)

An FEI Tecnai F20 XT Transmission Electron Microscope operated at 200 kV was used to characterize the morphology of the CN_x catalysts. Catalysts were prepared for imaging by suspending the catalyst in ethanol and then depositing the catalyst suspension on a lacey-formvar carbon supported on a 200 mesh copper TEM grid.

2.4. X-ray photoelectron spectroscopy

X-ray photoelectron spectroscopy (XPS) was used to study the surface chemical species on the CN_x catalysts. A Kratos Ultra Axis Spectrometer was used with a monochromated aluminum anode source. A complete survey spectrum, as well as spectra for the regions for O 1s, N 1s, C 1s, and S 2p was collected for each catalyst sample. Sensitivity factors reported for the anode and position by the manufacturer were used in the calculation of surface composition on the catalysts. Spectra baselines were determined using Shirely-type background fitting. Spectra were deconvoluted using Lorentzian-Gaussian combination peaks.

2.5. Hydrophobicity testing

The relative hydrophobicity of the CN_x catalysts was examined by suspending 1 mg of catalyst in 5 mL of DI water. The suspensions were sonicated for 30 min and then visually compared.

2.6. Temperature programmed oxidation experiments

Temperature programmed oxidation (TPOs) experiments were performed using a Setaram 111 TGA/DSC (theromogravimeteric analyzer/differential scanning calorimeter) instrument coupled to a MKS Cirrus residual gas analyzer to monitor the oxidation temperature and composition of the CN_x catalysts. For the TPO experiments, approximately 5 mg of CN_x was loaded into the TGA. The temperature was ramped at 5 °C/min to 750 °C while flowing 10% O_2/He. Product gas mass signals from 1–100 were monitored.

2.7. Temperature programmed desorption–temperature programmed oxidation experiments

Temperature programmed desorption (TPD)–temperature programmed oxidation (TPO) coupled experiments were performed using a Micromeritics Autochem II system coupled to a MKS Cirrus residual gas analyzer to study the CN_x catalyst surface and bulk species, as well as, the stability of the catalyst species. TPD–TPO experiments were performed with approximately 25 mg of catalyst. A helium gas stream was flowed over the catalyst bed while heating at 5 °C/min to 900 °C and cooling using forced convection back to room temperature for the TPD portion of the experiment. Following the TPD, a TPO was immediately ran in 5%O_2/He at 5 °C/min to 750 °C to characterize the catalyst material remaining after the TPD. The product gas mass signals of the entire experiment were monitored from 1–100.

To study the effect of the presence of water on the catalyst, 10 mol% water vapor was introduced into the TPD temperature ramp to 900 °C. The catalyst bed was cooled in He and then a TPO was performed as described above for the dry TPD–TPO experiment. The experiments involving water during the TPD are named wet-TPD–TPO experiments.

2.8. Oxygen reduction reaction activity and selectivity testing

Rotating ring disk electrode (RRDE) half-cell testing was performed on the catalysts to study the oxygen reduction reaction (ORR) activity and selectivity of the CN_x catalysts prepared. A PAR Bistat connected to a model 636 RRDE setup was used for the testing. The half-cell solution used was 0.5 M H_2SO_4. The choice of electrolyte was deemed acceptable for CN_x-based catalysts based upon reports in the literature that showed no significant change in catalyst testing results for carbon-nitrogen catalysts between H_2SO_4 and $HClO_4$ electrolytes [6,48]. An Ag/AgCl(sat KCl) reference electrode and a Pt wire counter electrode were used in the system. All potentials reported in this paper are referenced versus the normal hydrogen electrode (NHE).

Catalyst inks were prepared fresh for each RRDE test using a composition of 1:10:160 (by mass) catalyst: 5% Nafion in aliphatic alcohols: ethanol. Inks were sonicated for 30 min prior to applying three-5 μL aliquots of ink to the 0.1642 cm^2 glassy carbon disk, resulting in a catalyst loading of 426 $\mu g/cm^2$.

Catalyst testing was performed using cyclic voltammetry (CV) on the disk while monitoring any hydrogen peroxide products with the platinum ring held at a constant potential of 1.2 V vs. NHE. All CVs were scanned from 1.2 V to 0.0 V to 1.2 V vs. NHE. To begin testing, the electrolyte was saturated with oxygen and CVs were run at 10 mV/s to remove any gaseous oxygen from the catalyst pores and fully wet the catalyst. To collect a background, the half cell was purged with Argon to remove oxygen. CVs were run at a scan rate of 50 mV/s paired with the ring held at constant potential until scans were repeatable in Ar. Then a CV was run at 10 mV/s paired with the ring while rotating at 100 rpm to collect the background. The electrolyte was then saturated with oxygen to determine activity and selectivity of the catalysts. Once again CVs were run at 50 mV/s while holding the ring at constant potential until scans were repeatable. A scan in oxygen-saturated electrolyte was performed 100 rpm while holding the ring at 1.2 V vs. NHE. The scan rate was 10 mV/s. Additional CVs were run at 0 rpm and 1000 rpm in oxygen-saturated electrolyte using a scan rate of at 10 mV/s.

ORR activity is reported as the onset of activity, or where the oxygen-saturated CV current becomes greater than the argon-saturated background CV current when the CVs are scanned at 10 mV/s.

Possible reactions occurring on the catalyst include the desired water formation at [49]:

$$O_2 + 4e^- + 4H^+ \rightarrow 2H_2O \quad E^\circ = 1.23\,V \ vs.\ NHE$$

and the undesired hydrogen peroxide formation at [49]:

$$O_2 + 2e^- + 2H^+ \rightarrow H_2O_2 \quad E^\circ = 0.695\,V \ vs.\ NHE$$

The ring held at 1.2 V vs. NHE can detect hydrogen peroxide through the reaction [49]:

$$H_2O_2 \rightarrow O_2 + 2e^- + 2H^+ \quad E^\circ = -0.695\,V \ vs.\ NHE$$

Selectivity of the catalyst is reported as n, the number of electrons transferred per oxygen molecule. This is calculated by comparing the ring current (I_R), corrected for collection efficiency (N), to the disk current (I_D) using the following equation:

$$n = \frac{4I_D}{I_D + (I_R/N)}$$

An n value of 4.0 is equivalent to 100% selectivity towards water formation, while an n value of 2.0 is equivalent to 100% selectivity towards hydrogen peroxide formation. The collection efficiency was reported by the manufacturer as $N = 0.22$. This collection efficiency was verified for the system studied using a potassium ferricyanide redox couple. The experimental collection efficiency was found to be 0.214 ± 0.01 which is very close to the theoretical result reported by the manufacturer considering some have experienced 5% variability in their collection efficiency measurements [50,51].

RRDE selectivity was verified using the Koutecky–Levich technique using the same electrode and catalyst application method described for ORR activity testing. A series of cyclic voltammograms were acquired at 5 mV/s from 1.2 to 0.0 to 1.2 V vs. NHE in oxygen-saturated 0.5 M H_2SO_4 at 100, 200, 400, 900, 1600 rpm. Selectivity was determined by measuring the current density at several rotation rates using the Koutecky–Levich equation [49].

$$\frac{1}{j} = \frac{1}{j_k} + \frac{1}{B\omega^{1/2}}$$

$$B = 0.62nFC_{O_2}(D_{O_2})^{2/3}\nu^{-1/6}$$

where j is the current density (A/cm^3), j_k is the kinetically controlled current density, n is the number of electrons transferred per molecule of oxygen, F is Faraday's constant, C_{O_2} is the O_2 concentration in the electrolyte (1.1e−6 mol/cm^3 [52]), D_{O_2} is the diffusion coefficient for molecular oxygen in 0.5 M H_2SO_4 at 25 °C (1.4e−5 cm^2/s [52]), ν is the kinematic viscosity of the 0.5 M H_2SO_4 solution at 25 °C (0.01 cm^2/s [53]). The angular rotation rate in radians per second is represented as ω. The number of electrons transferred per oxygen molecule (n) can be determined from the slope of the linear relation of $1/j$ and $1/\omega^{1/2}$. The linearity and near parallelism of these plots indicates that the reaction follows first order kinetics.

3. Results and discussion

3.1. Thiophene as a growth promoter

The addition of thiophene into the acetonitrile pyrolysis feed stream did promote the deposition of carbon. At all thiophene growth promoter levels studied, sample weight gain during pyrolysis was greater than acetonitrile-only pyrolysis. As shown in Fig. 1, carbon deposition during pyrolysis goes through a maximum with increasing thiophene % in the feed mixture and the

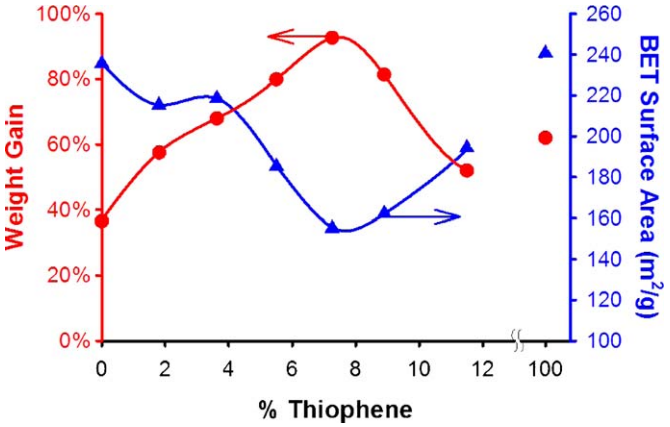

Fig. 1. Weight gain during pyrolysis of catalysts made with thiophene:acetonitrile combinations ($y1$-axis, circles) and the BET surface area of those materials ($y2$-axis, triangles).

maximum occurs at 7.3% thiophene concentration. This shows that sulfur, in the form of thiophene, can act as a growth promoter when the feed stream contains both carbon and nitrogen in the form of acetonitrile. Previous studies using thiophene and other sulfur-containing growth promoters have been for non-heteroatom containing carbon nanostructures. Even when thiophene was used as the only carbon precursor, significant amounts of carbon deposition occurred, indicating that thiophene does not inhibit the carbon deposition process even at high levels.

Interestingly, there was an inverse relationship between the amount of carbon deposition and the BET surface area of the catalysts, also shown in Fig. 1. This decrease in surface area could be caused by several reasons including the carbon nanostructure changing with growth promoter concentration or carbon depositing on itself reducing the amount of exposed surface.

3.2. Catalyst morphology

To determine the impact of the use of thiophene as a growth promoter on the morphology of the CN_x catalysts, TEM imaging was performed. CN_x catalysts made with no sulfur growth promoters grown over 2 wt%Fe/MgO produce mainly stacked cup nanofibers with varying diameters as shown in Fig. 2a. These stacked cup nanofibers have graphite edge planes exposed at an acute angle to the longitudinal axis. Also, as previously reported, all CN_x catalysts grown using a magnesia support contained some nanocubes, regardless of the metal on the support [35,37]. This observation held for these CN_x catalysts as well, though there were significantly more nanofibers than nanocubes.

When the lowest level of thiophene growth promoter was used, 1.8% (Fig. 2b), the morphology of the CN_x catalyst still remained mostly stacked cup nanofibers. There were more of the larger, less organized nanofibers and more nanocubes were also found compared to the thiophene-free catalyst. At the highest levels of growth promotion (7.3% thiophene), the catalyst morphology was no longer dominated by the stacked cup nanofibers (Fig. 2c). There were many more of the large, disordered nanofibers and a significant amount of nanocubes. Only a few stacked cup nanofibers were found. The change in morphology distribution along with the maximum growth promotion for the catalyst made with 7.3% thiophene may signify a change in the growth mechanism of the carbon deposition with higher thiophene contents. In comparison, the catalyst made with thiophene only (Fig. 2d) was composed of only nanocubes, indicating that acetonitrile was the precursor required to form stacked cup nanofibers over 2 wt%Fe/MgO fiber growth catalysts. Others have also observed changes in morphology with increased growth promoter concentration, as well, though the sulfur source and treatment conditions dictated whether changes observed were desirable or undesirable for the specific application [42,44,46].

3.3. Activity and selectivity testing

Activity and selectivity testing using the rotating ring disk electrode technique was performed on the CN_x catalysts manufactured using the growth promoter to determine if the use of thiophene had an impact on the catalyst performance for ORR. The catalyst made with acetonitrile only had an onset of activity at 760 mV vs. NHE. All catalysts made with pyrolyzing thiophene and acetonitrile combined had onsets of activity within a very tight range, near to that of the catalyst prepared with acetonitrile only, as shown in Fig. 3. The deviations in onset of activity measurements for these catalysts are not considered significant enough to distinguish differences in ORR activity. When thiophene was used as the only feedstock for the carbon growth, the ORR activity was very low. The onset of activity for the CS_y catalyst was 510 mV vs. NHE, which would be considered a very poor catalyst for ORR. The inset to Fig. 3 illustrates the significant difference with a voltammogram comparison of the CS_y catalyst (no acetonitrile) to CN_x(8.9). From the activity testing, it appears that as long as the catalyst precursor contained some amount of acetonitrile, the ORR activity could remain unchanged. Selectivity calculations obtained from RRDE testing found the selectivity of the CN_x-thiophene catalysts to range from an average of 3.6 to 3.9 electrons transferred per oxygen molecule. No trend in the selectivity of the catalysts with thiophene precursor content was observed.

There have been studies in the literature about the reliability of the RRDE technique for selectivity measurements [51,54–58]. It has been reported in the literature [51,57,58] and demonstrated in our laboratory that selectivity determined by RRDE is dependent upon the catalyst loading on the electrode disk. In this study, the catalyst loading was kept constant at 426 $\mu g/cm^2$.

To verify the selectivity results obtained by the RRDE technique, additional analysis using the Koutecky–Levich (K–L) Equation was performed on some of the catalysts. Fig. 4 is an example of the graphical results that were obtained from the Koutecky–Levich analysis for the CN_x (no thiophene) catalyst. K–L analysis results were comparable to those obtained by the RRDE, (n = 3.7 from K–L analysis as compared to a selectivity of n = 3.63 from RRDE measurements). It should be noted that the Koutecky–Levich analysis is not without its own shortcomings [59–62], but the comparison between the two methods provides additional confidence in the reported selectivity values.

Factors affecting selectivity of the CN_x-thiophene catalysts will be discussed further in Section 3.5.

3.4. Hydrophobicity testing

Relative hydrophobicity tests were performed by dispersing the catalysts in water with sonication. The use of thiophene as a growth promoter did not change the hydrophobicity/philicity properties of the catalysts as long as acetonitrile was still in the feed stream. An example of the hydrophobicity differences between catalysts made with acetonitrile and with thiophene-only is shown in Fig. 5. Carbon nanostructures grown using thiophene only are considerably more hydrophobic as can be seen from the lack of dispersion in water. This observation is consistent with the lack of edge planes observed over these materials (as confirmed through TEM) and could be linked to the differences in the activity of CN_x catalysts grown with or without the sulfur growth promoter and the CS_y materials.

3.5. Surface species characterization

X-ray photoelectron spectroscopy was used to characterize the surface species on the catalysts produced. The S 2p region was scanned to determine if there was any detectable sulfur, and if so, what type of sulfur species were present on the surface of the CN_x catalysts using thiophene as a growth promoter. Previous reports in the literature focus on the growth promotion effects of sulfur, but do not extensively discuss the sulfur that could be incorporated into the product carbon nanofibers [42–47]. The impact of the presence of sulfur in the nanofiber could be significant depending upon the application. XPS analysis showed that there was a significant amount of sulfur on the nanostructure surfaces. Surface sulfur content for the CN_x-thiophene catalysts ranged from 0.7 to 1.6 atomic%, as shown in Table 1. The catalyst prepared using 100% thiophene (CS_y) had 3.6% sulfur on its surface. Fig. 6a shows the S 2p region for a representative group of the CN_x-thiophene and CS_y catalysts. Up to three types of sulfur can be identified in these catalysts. The peak at 168.3 eV was attributed to sulfate species [63,64]. The literature has some discrepancies in the assignment of

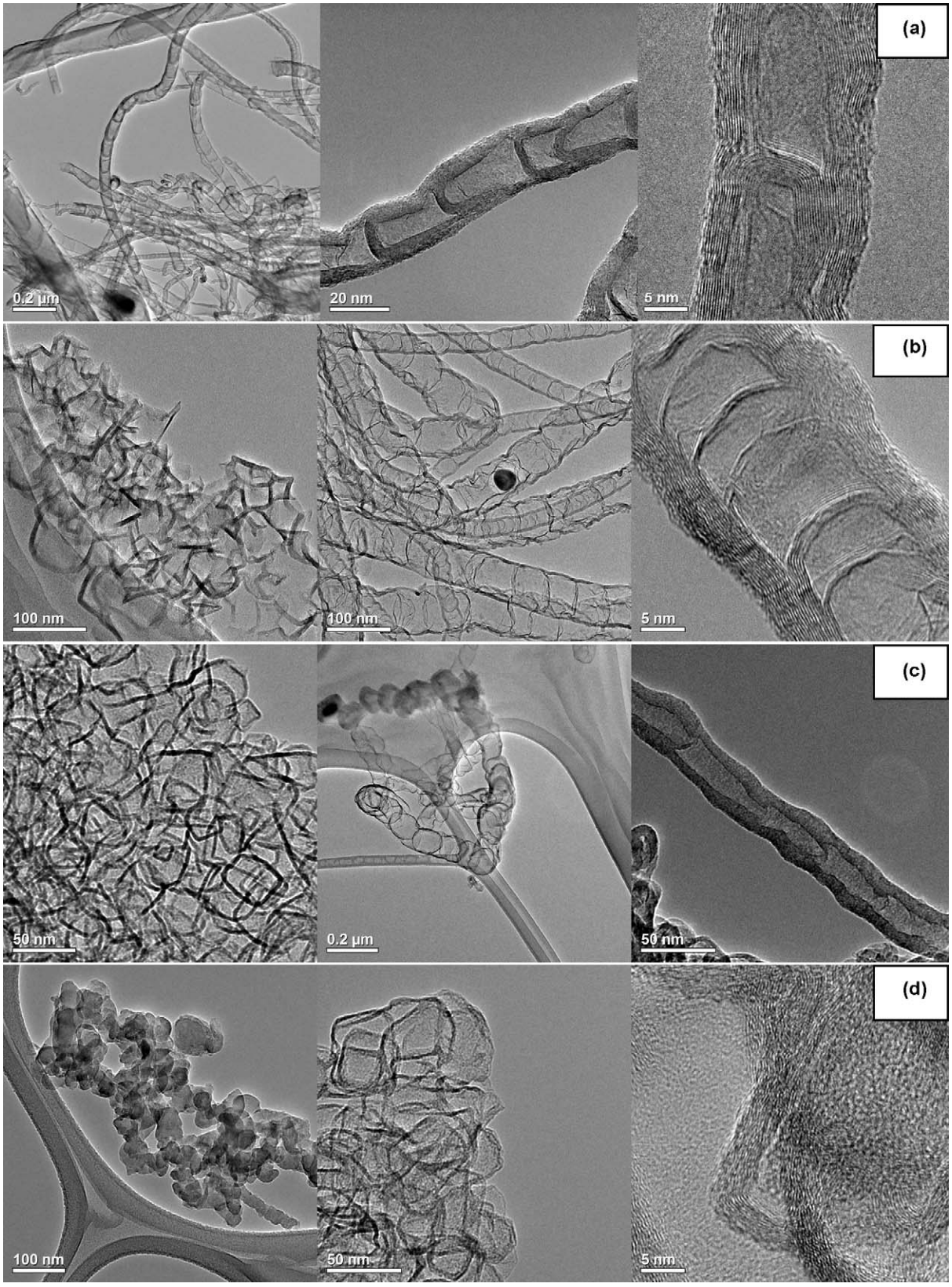

Fig. 2. TEM images of (a) CN_x–no thiophene, (b) CN_x–1.8% thiophene, (c) CN_x–7.3% thiophene, (d) CS_y–100% thiophene.

sulfur species in the 163–164 eV region. Fig. 6a shows one doublet being fitted to the 163–164 eV envelope. S-C species can be identified at 163.5 eV [63,65,66]. The peak at 164.1 eV was assigned to elemental sulfur [63,66]. The assignment of C-S is less certain, as some have identified C-S at 163 eV [65], while others attributed 163.6 eV peak to possibly S-S or S-C [66] and 163.6 eV to only S-S [63]. Fig. 6b is an example of when two doublet peaks are fitted in the 163–164 eV envelope. Both fits are reasonably good and possible. It is possible that both elemental S and S-C species are present in the thiophene-CN_x catalysts with

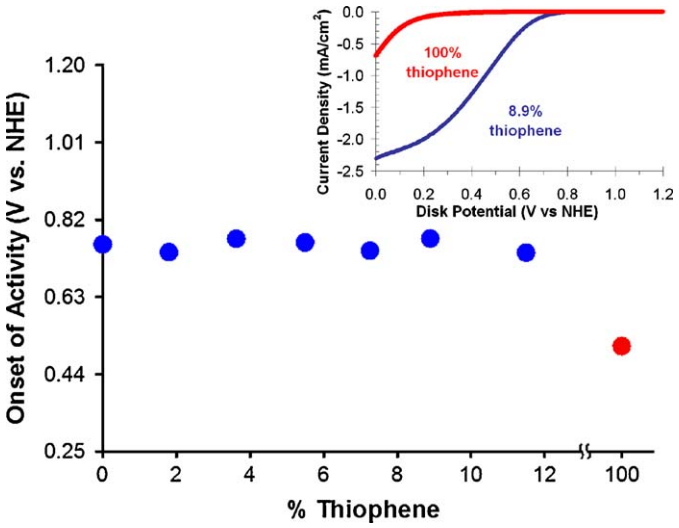

Fig. 3. Onset of activity comparison for thiophene containing catalysts. Inset: Activity comparison of the linear scan at 1000 rpm in oxygen-saturated 0.5 M H_2SO_4 for CN_x–8.9% thiophene and 100% thiophene catalysts.

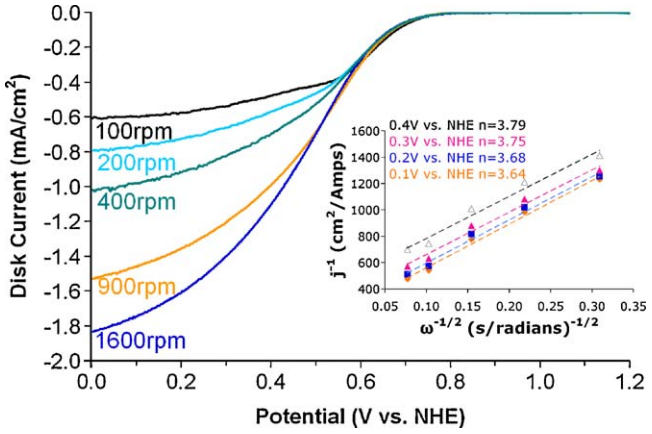

Fig. 4. Linear scans at 5 mV/s as a function of rotation rate on CN_x–no thiophene in oxygen-saturated 0.5 M H_2SO_4. Inset: Koutecky–Levich analysis for this catalyst.

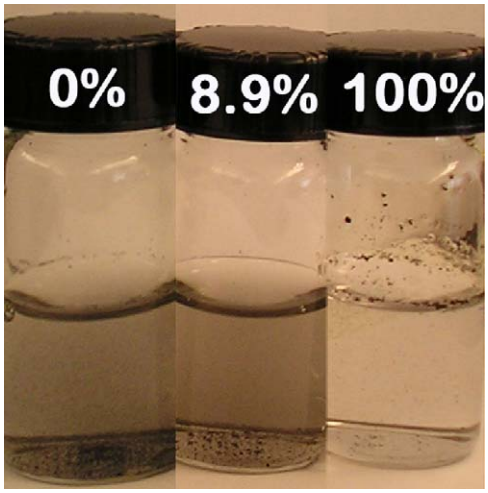

Fig. 5. Hydrophobicity comparison of CN_x, CN_x(8.9%) and CN_y catalysts showing their dispersion in water.

Table 1
Surface composition of catalysts from XPS.

%Thiophene in acetonitrile	0%	1.8%	3.6%	5.5%	8.9%	11.5%	100%
O 1s	1.9	10.0	8.6	5.4	15.4	6.1	8.0
N 1s total	9.3	7.6	7.4	8.3	7.7	7.2	0.0
Pyridinic	26.1	26.7	27.3	23.7	31.4	23.7	0.0
Quartenary	47.8	47.9	47.8	49.4	45.6	48.6	0.0
Pyridinic-N-O	26.1	25.4	24.9	27.0	23.0	27.8	0.0
C 1s	88.8	81.7	82.7	85.4	75.2	85.9	88.9
S 2p	0.0	0.7	1.4	1.0	1.6	0.9	3.1

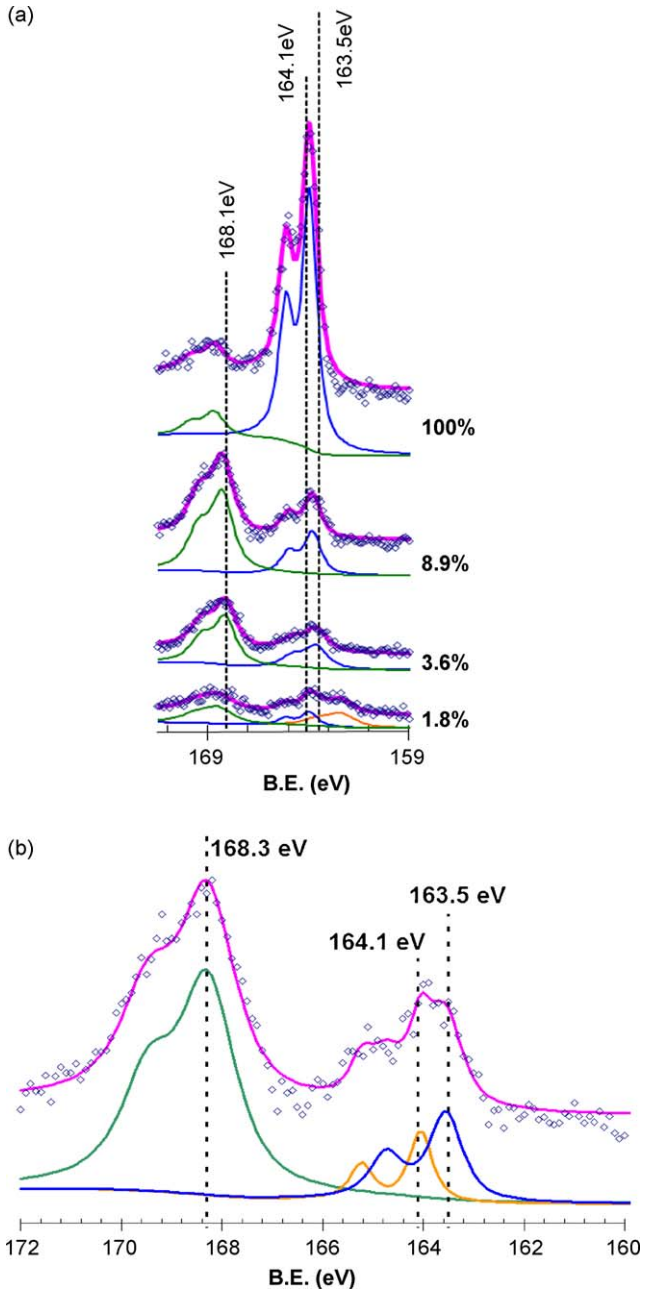

Fig. 6. (a) XPS S 2p region for selected CN_x–thiophene catalysts (labels are mol% thiophene in acetonitrile solution) deconvoluted using two doublets, (b) XPS S 2p region deconvoluted using three doublets for CN_x–8.9%thiophene.

excess elemental sulfur being present on the surface of the catalyst. The sulfate identified could have been elemental sulfur that, when exposed to air, reacted to form sulfate. This is possible, as the samples are exposed to air after they are synthesized. Interestingly,

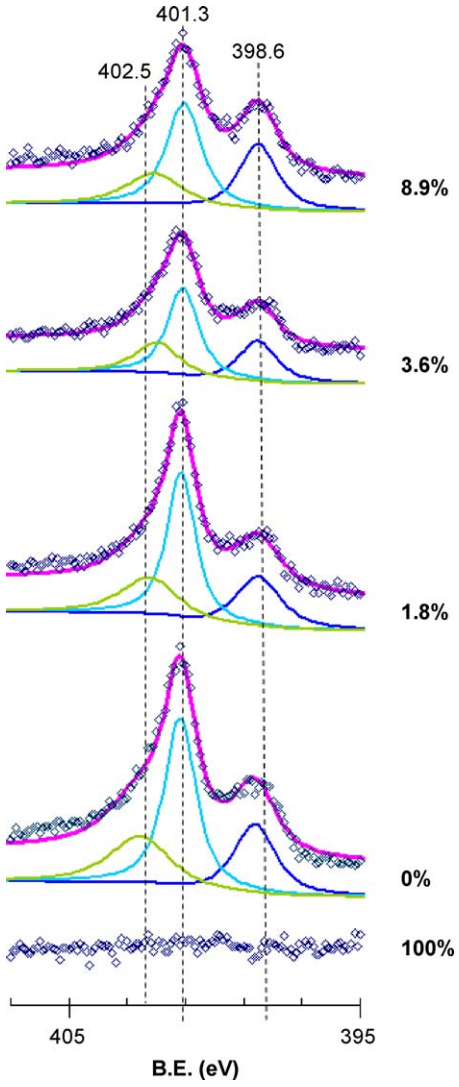

Fig. 7. XPS N 1s region deconvoluted for select CN_x–thiophene catalysts (labels are mol% thiophene in acetonitrile solution).

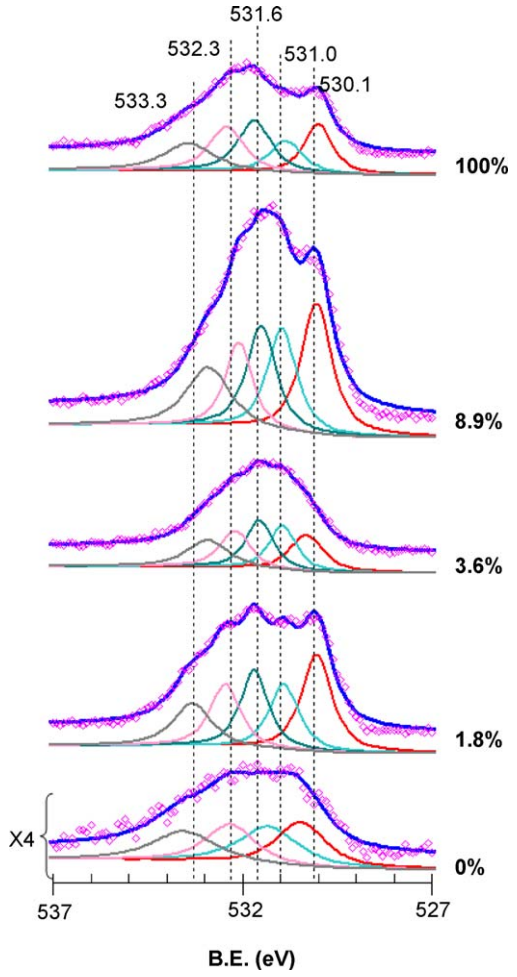

Fig. 8. XPS O1s region deconvoluted for select CN_x–thiophene catalysts (labels are mol% thiophene in acetonitrile solution).

the fitting of the CN_x(1.8%) catalysts required an additional lower binding energy doublet. This species has not been identified at this time, but sulfides are commonly found in this region.

X-ray photoelectron spectra of the N 1s region for the CN_x-thiophene catalysts were examined to determine if the introduction of sulfur led to significant changes in the nature or the quantity of the detected surface nitrogen species (Fig. 7). CN_x catalysts grown with acetonitrile only over 2 wt%Fe/MgO contained 9.3% nitrogen with the nitrogen content being split into 26.1% pyridinic-N (located on the graphitic edge planes), 47.8 quarternary-N (located inside the graphitic plane), and 26.1% pyridinic-N-O, as shown in Table 1. These results are similar to what has previously been observed in our research for CN_x catalysts grown over Fe/MgO supports [35]. When thiophene was used as a growth promoter, the nitrogen level dropped to between 7 and 8 atomic%. The breakdown of the nitrogen species changed little with the introduction of thiophene into the pyrolysis feed stream, as shown in Table 1 and in Fig. 7. This relatively high amount of nitrogen and limited change to the nitrogen species most likely contributes to why no significant change in ORR activity for these catalysts was observed. It also suggests that the presence of thiophene does not alter the mechanism for incorporation of nitrogen into the graphite structure through

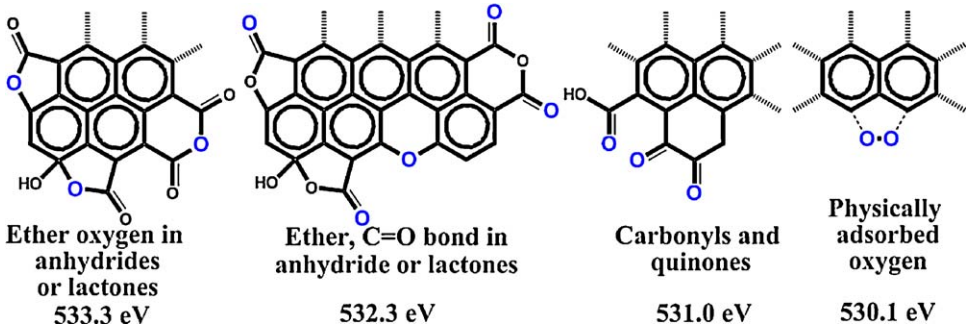

Fig. 9. Locations of possible oxygen functional groups (indicated by large blue O) by XPS binding energy.

acetonitrile pyrolysis. The absence of any detectable nitrogen in the CS_y may also explain why it was relatively inactive for ORR.

XPS analysis showed that the oxygen content increased significantly with the use of thiophene as a growth promoter. Oxygen content went from under 2 atomic% of the surface when no thiophene was used to more than 15% when 8.9% thiophene was introduced into the feed stream. While some of the oxygen content can be attributed to the sulfate species formation, the contribution from sulfate in the O 1s region does not account for all of the oxygen increase. It appears that the presence of sulfur may promote the addition of oxygen species onto the carbon. Five types of oxygen were identified from the O 1s spectra, as deconvoluted on representative catalysts in Fig. 8. These species can be identified as physically adsorbed oxygen at 530.1 eV [67]; carbonyls and quinones at 531.0 eV [64,68]; sulfur–oxygen compounds at 531.6 eV [69]; ethers, and C=O in anhydrides or lactones at 532.3 eV [64,68]; and ether oxygens in anhydrides or lactones at 533.3 eV [64,68]. A peak fit with fewer curves fails to recognize oxygen-sulfur species and quinone species, although we have evidence of their presence from XPS (S 2p region) and electrochemistry testing. The full width half-maximum (FWHM) of the peaks remains reasonable at about 1 eV on all of the fits using five curves and have peak locations that match multiple literature reports well. The typical oxygen species found in graphite and their binding energy assignments are shown in Fig. 9. The composition fractions changed little with sulfur content, with each component making up 15–25% of the oxygen spectra, this may also be due to the combination of oxygen species identified in the literature at each binding energy.

While no trend in selectivity with thiophene concentration or resulting sulfur content of the catalysts was observed, a trend in selectivity with oxygen surface content was observed. Selectivity of the catalysts increased with oxygen content as shown in Fig. 10a where the oxygen content was normalized for the surface area of the catalysts. The inset to Fig. 10a is a visual comparison of the ring current (corrected for collection efficiency) to the absolute disk current. A series of curves used in the calculation of the selectivity of the catalyst from RRDE testing is shown in Fig. 10b. Due to the fairly even distribution of types of oxygen species on the catalyst surface, no one type of oxygen (from XPS results) was found to control the selectivity trend with oxygen functionalization. The presence of oxygen may contribute to the complete formation to water. This was also observed on the CN_x catalysts in a separate study when they were treated with nitric acid to add oxygen functional groups [70]. Some researchers have hypothesized that the quinone/hydroquione groups play a role in oxygen reduction [28,71], though no clear trend in our study was observed with the quinone groups when comparing them to the selectivity of the catalysts found.

3.6. Stability of sulfur in CN_x nanostructures

Once it was determined that thiophene could be used as a growth promoter for CN_x and that the ORR activity was not affected by the presence of sulfur in the final CN_x product, further studies were performed to examine if sulfur species might elute under conditions that would be relevant to an actual fuel cell environment. RRDE testing does not readily reveal the ability of a catalyst to withstand the fuel cell environment for long durations without activity loss, material degradation, or leaching of the catalyst components into other parts of the fuel cell. To address the preliminary concerns of degradation and leaching, temperature programmed oxidation (TPO) and temperature programmed desorption (TPD) experiments were performed. In addition, desorption tests were also performed in the presence of water to mimic the humidified conditions of a fuel cell environment better.

The temperature at which significant oxidation of carbon materials begins can be a marker for the orderliness of the material and can imply what the oxidation resistance over long periods of time may be for the material. In addition, the chemical species that are evolved during oxidation indicates the chemical composition of the material. TPO experiments were performed in a TGA-DSC instrument connected to a mass spectrometer for product analysis. It was found that all CN_x-thiophene catalysts had similar oxidation properties to CN_x made without thiophene, as shown by the TG signal in Fig. 11a. Significant oxidation of these catalysts began at about 485 °C. While the largest mass loss occurred for the CS_y

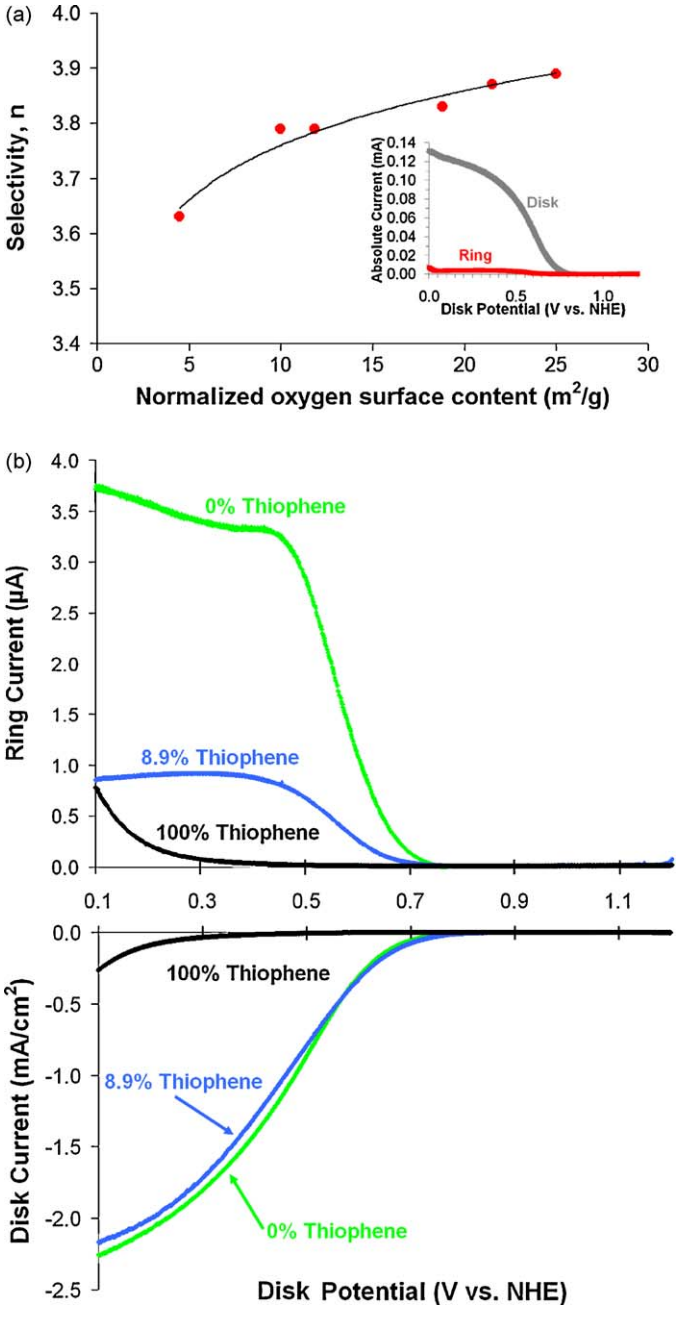

Fig. 10. (a) Selectivity, *n*, (number of electrons transferred per oxygen molecule) from RRDE as a function of normalized oxygen surface content. Inset: Visual comparison of disk (absolute current) to ring (after adjustment for theoretical collection efficiency) currents at 100 rpm in oxygen-saturated 0.5 M H_2SO_4 for CN_x–8.9%thiophene. (b) Comparison of ring to disk currents used in determination of selectivity from RRDE. System is oxygen-saturated 0.5 M H_2SO_4 with background currents subtracted for both ring and disk.

catalyst at the same temperature as the CN_x-thiophene catalysts, an initial mass loss of 18% was observed beginning at about 220 °C. From the mass spectrometry data collected at the outlet of the reaction, a significant SO_2 peak was observed for the CS_y catalyst during the 18% mass loss region (Fig. 11b). The other catalysts made with varying levels of thiophene also had SO_2 evolved at this temperature, but with signal intensities more than an order of magnitude smaller than the 100% thiophene catalyst. This small amount of SO_2 evolution on the CN_x-thiophene catalysts did not cause significant mass loss due to the minimal amount evolved. During the oxidation period beginning at about 485 °C, carbon oxidation, nitrogen oxidation and sulfur oxidation products were observed in the product gas analysis. It was observed that CO_2 evolved earlier than the NO_x and SO_2 during the final oxidation stage. Carbon that was less graphitized or contained more defects may begin the oxidation process before the more ordered carbon [72]. From the product analysis, it appears that the nitrogen and sulfur imbedded in the carbon came more from the latter type of carbon. Overall, the TPO results suggest that there are two types of sulfur in the CN_x-thiophene and CS_y catalysts–sulfur that was easily evolved from the surface and sulfur that was incorporated into the carbon matrix.

To further study the two types of sulfur observed and to evaluate the desorption properties of the catalysts, TPD experiments were performed on the CN_x-thiophene catalysts that were immediately followed by TPOs. From these TPD experiments where the temperature was ramped in He to 900 °C before cooling under the same atmosphere, a sulfur desorption peak was observed that began at about 175 °C and ended about one hundred degrees later (an illustration of this is shown for the CN_x-3.6%thiophene catalyst experiment in Fig. 12a). This peak

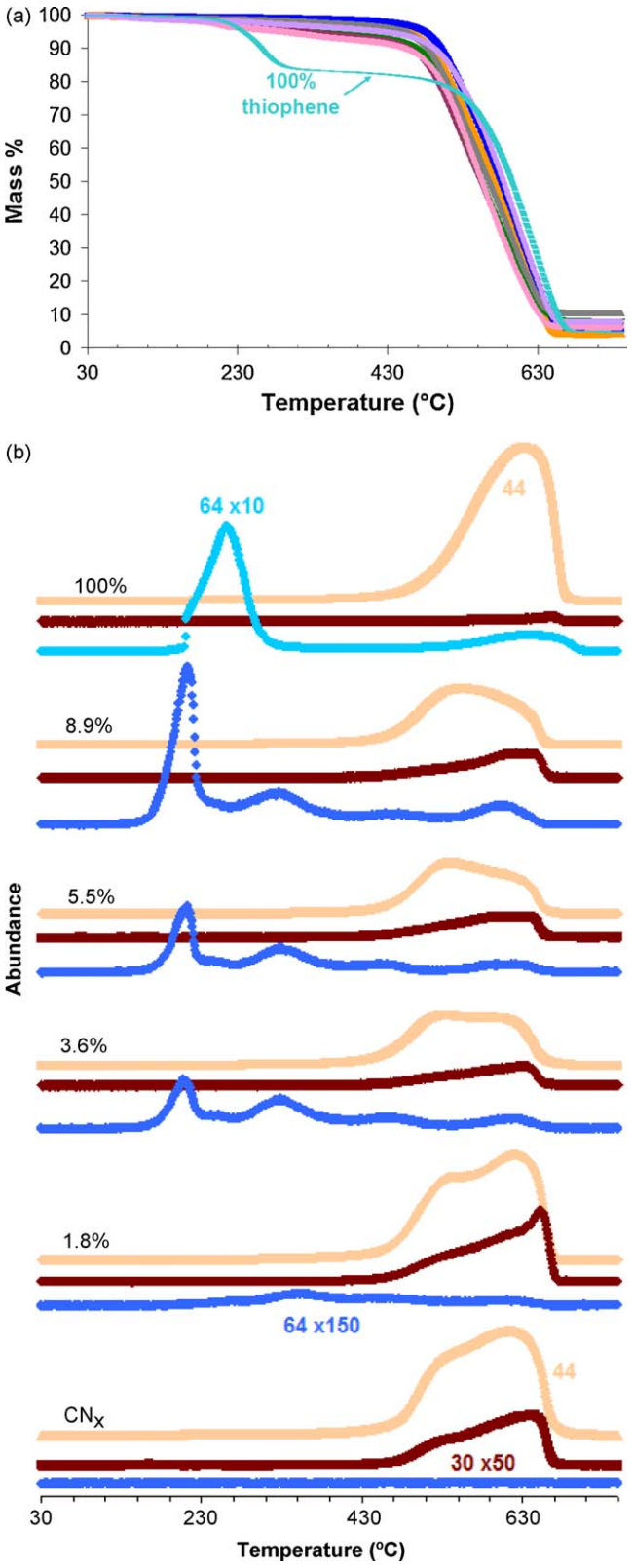

Fig. 11. TPO experiments ran in 10%O_2/He (a) TG signal, (b) Mass signals for 44 (CO_2), 30 (×50) (NO_x), and 64 (×150 for CN_x–1.8%, 3.6%, 5.5% and 8.9% thiophene; ×10 for 100% thiophene catalyst) (SO_2).

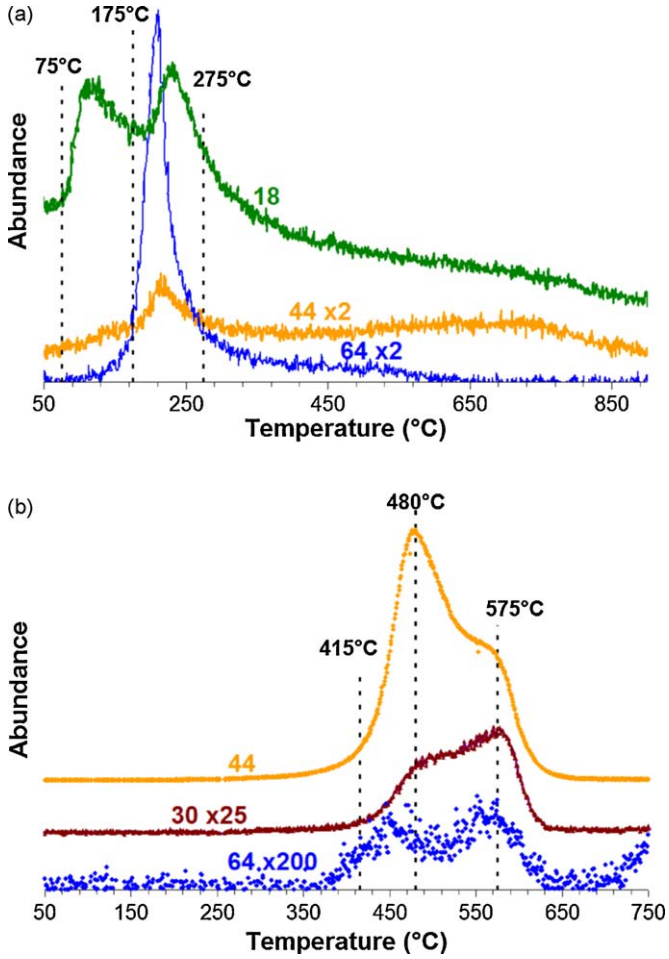

Fig. 12. TPD-TPO experiment for CN_x–3.6% thiophene (a) TPD in He showing mass signals 18 (H_2O), 44 (CO_2) and 64 (SO_2), b) TPO in 5%O_2/He showing mass signals 30 (NO_x), 44 (CO_2) and 64 (SO_2).

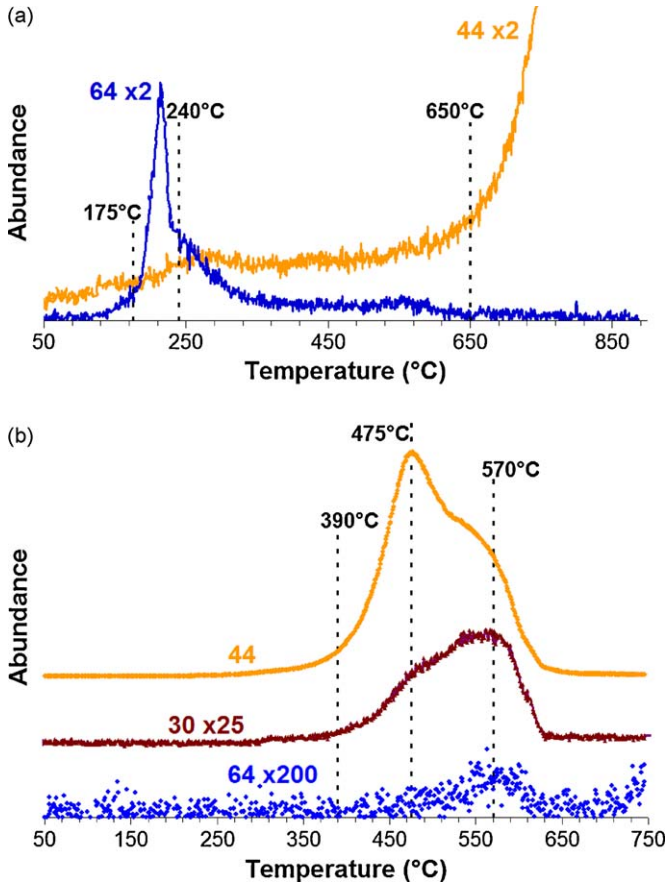

Fig. 13. Wet-TPD-TPO experiment for CN_x–3.6% thiophene (a) wet-TPD in 10%H_2O/He showing mass signals 44 (CO_2) and 64 (SO_2), (b) TPO in 5%O_2/He showing mass signals 30 (NO_x), 44 (CO_2) and 64 (SO_2).

corresponds well to the sulfur peak observed during the TGA–TPO experiments discussed above, suggesting that the early sulfur evolution in the TPOs was due to the desorption of adsorbed sulfur on the surface of the catalyst. The TPO experiments that immediately followed the TPD also showed sulfur oxidation during the carbon oxidation (Fig. 12b). The information gained from the TGA–TPO and TPD–TPO experiments support the sulfur species identified by XPS, namely elemental sulfur, S-O and S-C. The elemental and S-O sulfur would be desorbed at lower temperatures and the sulfur which was incorporated into the graphite matrix, i.e., S-C, was only released during the carbon oxidation.

While TPD–TPO experiments were useful in verifying the types of sulfur species present in the CN_x-thiophene catalysts and the temperatures at which sulfur began to evolve from the surface of the catalyst, the impact of the high-humidity fuel cell environment may alter these properties, especially the desorption temperatures. To address this, TPD experiments were repeated by introducing 10% water into the He feed stream during temperature ramping to 900 °C (labeled "wet-TPD"). Wet-TPD experiments were followed by TPO after the catalyst was cooled in He. It was found that sulfur desorption was not significantly affected by the presence of water. As shown in Fig. 13a, the desorption of sulfur began at about the same temperature as when it did in dry conditions. Also, to be noted from the wet-TPD was that water began to oxidize the CN_x catalysts at about 700 °C. The TPO immediately following the TPD (shown in Fig. 13b) also did not show any early sulfur desorption, indicating that all adsorbed sulfur on the surface of the catalyst was removed during the initial heat ramp. During the carbon oxidation stage, small quantities of SO_2 were still observed. The temperatures of the sulfur desorption and carbon oxidation in both the presence of water and the presence of oxygen are significantly higher than the operating temperatures for PEM and DMFC of 60–80 °C. This should limit the amount of sulfur desorption into the fuel cell and carbon oxidation during operation. Pretreatments of the catalyst could also be performed to reduce the risk of any sulfur contamination.

4. Conclusions

It was shown that thiophene can be used as a growth promoter in the acetonitrile pyrolysis production of CN_x catalysts for the oxygen reduction reaction. Low levels (2–5 mol%) of thiophene promote carbon deposition without significantly altering the carbon nanostructure. Even though sulfur was incorporated into the CN_x both as adsorbed elemental sulfur and its oxides or S-C, the ORR activity was not impacted. Selectivity of the catalyst to water formation was not a function of thiophene used as a growth promoter, but rather a function of the amount of oxygen functional groups present on the CN_x surface. The use of thiophene did increase the amount of oxygen functional groups present.

If the CN_x-thiophene catalysts were pretreated in an inert atmosphere at 250–300 °C, the adsorbed sulfur could be removed from the surface of the catalyst, significantly reducing the possibility of sulfur leaching into the fuel cell.

Acknowledgment

The authors gratefully acknowledge the support for this work from the U.S. Department of Energy–Basic Energy Sciences (DE-FG02-07ER15896).

References

[1] R. Jasinski, Nature 201 (1964) 1212.
[2] R. Jasinski, J. Electrochem. Soc. 112 (1965) 526–528.
[3] E. Yeager, Electrochim. Acta 29 (1984) 1527–1537.
[4] E. Yeager, J. Mol. Catal. 38 (1986) 5–25.
[5] M. Bron, S. Fletcher, M. Hilgendorff, P. Bogdanoff, J. Appl. Electrochem. 32 (2002) 211.
[6] S. Gojkovic, S. Gupta, R. Savinell, J. Electroanal. Chem. 462 (1999) 63–72.
[7] P. Gouerec, A. Biloul, O. Contamin, G. Scarbeck, M. Savy, J. Riga, L.T. Weng, P. Bertrand, J. Electroanal. Chem. 422 (1997) 61.
[8] H. Jahnke, M. Schonborn, G. Zimmerman, Fortschr. Chem. Forsch. 61 (1976) 133.
[9] K. Wiesener, Electrochim. Acta 31 (1986) 1073–1078.
[10] S. Gupta, D. Tryk, I. Bae, W. Aldred, E. Yeager, J. Appl. Electrochem. 19 (1989) 19.
[11] R. Cote, G. Lalande, D. Guay, J.P. Dodelet, G. Denes, J. Electrochem. Soc. 145 (1998) 2411.
[12] M. Lefevre, J.P. Dodelet, P. Bertrand, J. Phys. Chem. B 106 (2002) 8705–8713.
[13] F. Jaouen, S. Marcotte, J.-P. Dodelet, G. Lindbergh, J. Phys. Chem. B 107 (2003) 1376–1386.
[14] J. Maruyama, I. Abe, J. Electrochem. Soc. 154 (2007) B297–B304.
[15] E.B. Easton, A. Bonakdarpour, J.R. Dahn, Electrochem. Solid State 9 (2006) A463–A467.
[16] A. Garsuch, R. d'Eon, T. Dahn, O. Klepel, R.R. Garsuch, J.R. Dahn, J. Electrochem. Soc. 155 (2008) B236–B243.
[17] R. Bashyam, P. Zelenay, Nature 443 (2006) 63–66.
[18] G. Wei, J.S. Wainright, R.F. Savinell, J. New Mater. Electrochem. Sys. 3 (2000) 121–129.
[19] M. Bron, J. Radnik, M. Fieber-Erdmann, P. Bogdanoff, S. Fiechter, J. Electroanal. Chem. 535 (2002) 113–119.
[20] G. Lalande, R. Cote, D. Guay, J.P. Dodelet, L.T. Weng, P. Bertrand, Electrochim. Acta 42 (1997) 1379.
[21] M. Lefevre, J.-P. Dodelet, Electrochim. Acta 53 (2008) 8269–8276.
[22] F. Charreteur, F. Jaouen, S. Ruggeri, J.-P. Dodelet, Electrochim. Acta 53 (2008) 2925–2938.
[23] S. Ruggeri, J.-P. Dodelet, J. Electrochem. Soc. 154 (2007) B761–B769.
[24] F. Jaouen, M. Lefevre, J.-P. Dodelet, M. Cai, J. Phys. Chem. B 110 (2006) 5553–5558.
[25] F. Jaouen, F. Charreteur, J.P. Dodelet, J. Electrochem. Soc. 153 (2006) A689–A698.
[26] G. Gruenig, K. Wiesner, S. Gamburzev, I. Iliev, A. Kaisheva, J. Electroanal. Chem. 159 (1983) 155–162.
[27] R. Franke, D. Ohms, K. Wiesner, J. Electroanal. Chem. 260 (1989) 63–73.
[28] N.P. Subramanian, S.P. Kumaraguru, H. Colon-Mercado, H. Kim, B.N. Popov, T. Black, D.A. Chen, J. Power Sources 157 (2006) 56–63.
[29] P. Wang, Z. Ma, Z. Zhao, L. Jia, J. Electroanal. Chem. 611 (2007) 87–95.

[30] F. Charreteur, S. Ruggeri, F. Jaouen, J.P. Dodelet, Electrochim. Acta 53 (2008) 6881–6889.
[31] N.P. Subramanian, X. Li, V. Nallathambi, S.P. Kumaraguru, H. Colon-Mercado, G. Wu, J.-W. Lee, B.N. Popov, J. Power Sources 188 (2009) 38–44.
[32] T. Ikeda, M. Boero, S.-F. Huang, K. Terakura, M. Oshima, J.-i. Ozaki, J. Phys. Chem. C 112 (2008) 14706–14709.
[33] P.H. Matter, U.S. Ozkan, Catal. Lett. 109 (2006) 115–123.
[34] P.H. Matter, E. Wang, M. Arias, E.J. Biddinger, U.S. Ozkan, J. Phys. Chem. B 110 (2006) 18374–18384.
[35] P.H. Matter, E. Wang, M. Arias, E.J. Biddinger, U.S. Ozkan, J. Mol. Catal. 264 (2007) 73–81.
[36] P.H. Matter, E. Wang, J.-M.M. Millet, U.S. Ozkan, J. Phys. Chem. C 111 (2007) 1444–1450.
[37] P.H. Matter, E. Wang, U.S. Ozkan, J. Catal. 243 (2006) 395–403.
[38] P.H. Matter, L. Zhang, U.S. Ozkan, J. Catal. 239 (2006) 83–96.
[39] E.J. Biddinger, U.S. Ozkan, Top. Catal. 46 (2007) 339–348.
[40] K. Gong, F. Du, Z. Xia, M. Durstock, L. Dai, Science 323 (2009) 760–764.
[41] M. Lefevre, E. Proietti, F. Jaouen, J.-P. Dodelet, Science 324 (2009) 71–74.
[42] L. Ci, Y. Li, B. Wei, J. Liang, C. Xu, D. Wu, Carbon 38 (2000) 1933–1937.
[43] L. Ci, J. Wei, B. Wei, J. Liang, C. Xu, D. Wu, Carbon 39 (2001) 329–335.
[44] Y.-Y. Fan, H.-M. Cheng, Y.-L. Wei, G. Su, Z.-H. Shen, Carbon 38 (2000) 921–927.
[45] Y.-Y. Fan, H.-M. Cheng, Y.-L. Wei, G. Su, Z.-H. Shen, Carbon 38 (2000) 789–795.
[46] M.S. Kim, N.M. Rodriguez, R.T.K. Baker, J. Catal. 143 (1993) 449–463.
[47] N.M. Rodriguez, M.S. Kim, F. Fortin, I. Mochida, R.T.K. Baker, Appl. Catal. A-Gen. 148 (1997) 265–282.
[48] F. Jaouen, J. Herranz, M. Lefevre, J.-P. Dodelet, U.I. Kramm, I. Herrmann, P. Bogdanoff, J. Maruyama, T. Nagaoka, A. Garsuch, J.R. Dahn, T.S. Olson, S. Pylypenko, P. Atanassov, E.A. Ustinov, ACS Appl. Mater. Interf. 1 (2009) 1623–1639.
[49] A.J. Bard, L.R. Faulkner, Electrochemical methods: fundamentals and applications, John Wiley and Sons Ltd, New York, 2001.
[50] O. Antoine, R. Durand, J. Appl. Electrochem. 30 (2000) 839–844.
[51] A. Bonakdarpour, M. Lefevre, R. Yang, F. Jaouen, T. Dahn, J.-P. Dodelet, J.R. Dahn, Electrochem. Solid State 11 (2008) B105–B108.
[52] K.-L. Hsueh, E.R. Gonzalez, S. Srinivasan, Electrochim. Acta 28 (1983) 691–697.
[53] G. Baysinger, L.I. Berger, R.N. Goldberg, H.V. Kehiaian, K. Kuchitsu, G. Rosenblatt, D.L. Roth, D. Zwillinger, CRC Handbook of Chemistry and Physics, 74 ed., CRC Press, Boca Raton FL, 2005.
[54] R. Boulatov, in: J.H. Zagal, F. Bedioui, J.-P. Dodelet (Eds.), N_4-Macrocyclic Metal Complexes, Springer Science+Business Media, Inc, New York, 2006, pp. 1–40.
[55] J.H. Zagal, M.A. Paez, J.F. Silva, in: J.H. Zagal, F. Bedioui, J.-P. Dodelet (Eds.), N_4-Macrocyclic Metal Complexes, Springer Science + Business Median, Inc, New York, 2006, pp. 41–82.
[56] K.J.J. Mayrhofer, D. Strmcnik, B.B. Blizanac, V. Stamenkovic, M. Arenz, N.M. Markovic, Electrochim. Acta 53 (2008) 3181–3188.
[57] A. Bonakdarpour, T.R. Dahn, R.T. Atanasoski, M.K. Debe, J.R. Dahn, Electrochem. Solid State 11 (2008) B208–B211.
[58] A. Bonakdarpour, C. Delacote, R. Yang, A. Wieckowski, J.R. Dahn, Electrochem. Commun. 10 (2008) 611–615.
[59] Y.-H. Shih, G.V. Sagar, S.D. Lin, J. Phys. Chem. C 112 (2008) 123–130.
[60] M. Bron, S. Fiechter, P. Bogdanoff, H. Tributsch, Fuel Cells 2 (2003) 137–142.
[61] S. Mentus, Electrochim. Acta 50 (2004) 27–32.
[62] A. Altamirano-Gutierrez, O. Jimenez-Sandoval, J. Uribe-Godinez, R.H. Castellanos, E. Borja-Arco, J.M. Olivares-Ramirez, Int. J. Hydrogen Energy 34 (2009) 7983–7994.
[63] Y. Garsany, O.A. Baturina, K.E. Swider-Lyons, J. Electrochem. Soc. 154 (2007) B670–B675.
[64] G. Zhang, S. Sun, D. Yang, J.-P. Dodelet, E. Sacher, Carbon 46 (2008) 196–205.
[65] O. Contamin, C. Debiemme-Chouvy, M. Savy, G. Scarbeck, J. New Mater. Electrochem. Sys. 3 (2000) 67–74.
[66] X.-g. Yu, J.-y. Xie, J. Yang, H.-j. Huang, K. Wang, Z.-s. Wen, J. Electroanal. Chem. 573 (2004) 121–128.
[67] V. Datsyuk, M. Kalyva, K. Papagelis, J. Parthenios, D. Tasis, A. Siokou, I. Kallitsis, C. Galiotis, Carbon 46 (2008) 833–840.
[68] J.L. Figueiredo, M.F.R. Pereira, M.M.A. Freitas, J.J.M. Orfao, Carbon 37 (1999) 1379–1389.
[69] C.L. Bianchi, S. Ardizzone, G. Cappelletti, Surf. Interf. Anal. 36 (2004) 745–748.
[70] E.J. Biddinger, D. von Deak, U.S. Ozkan, Top. Catal. 52 (2009) 1566–1574.
[71] Y. Nabae, I. Yamanaka, K. Otsuka, Appl. Catal. A-Gen. 280 (2005) 149–155.
[72] K. Kinoshita, Carbon, Electrochemical and Physiochemical Properties, Wiley Interscience, New York, 1988.